ACS APPLIED MATERIALS & INTERFACES

Research Article

www.acsami.org

Adhesion Energy of MoS_2 Thin Films on Silicon-Based Substrates Determined via the Attributes of a Single MoS_2 Wrinkle

Shikai Deng,[†] Enlai Gao,[‡] Zhiping Xu,[‡] and Vikas Berry*[,†]

[†]Department of Chemical Engineering, University of Illinois at Chicago, 810 South Clinton Street, Chicago, Illinois 60607, United States

[‡]Applied Mechanics Laboratory, Department of Engineering Mechanics, Tsinghua University, Beijing 100084, China

Supporting Information

ABSTRACT: Understanding the energetics of adhesion between two-dimensional nanomaterials and their supporting substrates is crucial for the design and fabrication of correrresponding structures with controlled interfacial effects that influence phononics, charge-carrier distribution, and electronic response. Here, we show a mechanical energy model that equates the adhesion energy of MoS_2 on rigid and flat substrates (SiO_2 and Si_3N_4) to the attributes of a single wrinkle in a MoS_2 flake. The amplitude of the observed wrinkles was normalized for thickness (A/t) to select the wrinkles valid for the model. The adhesion energy values of 0.170 ± 0.033 J m^{-2} for MoS_2 on SiO_2 and 0.252 ± 0.041 J m^{-2} for MoS_2 on Si_3N_4 were determined. This mechanical energy model is consistent with the model based on the local equilibrium at the contact point in the Young's equation. We also propose a method to measure the plane-strain in wrinkled MoS_2. The geometrical properties (symmetry and normalized dimensions) of wrinkles and substrate effects are also discussed.

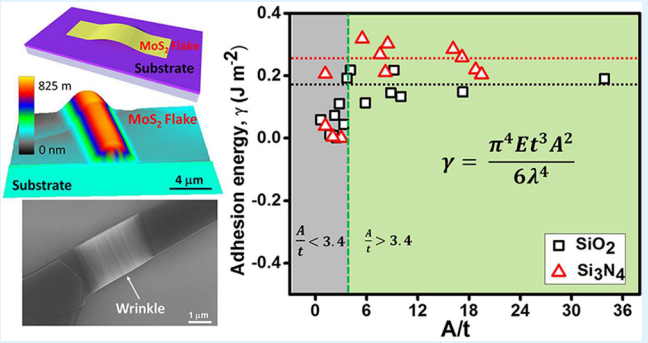

KEYWORDS: *adhesion energy, MoS_2, wrinkles, silicon dioxide, silicon nitride, strain*

INTRODUCTION

Flexible two-dimensional nanomaterials (2DNs), such as graphene, boron nitride, and transition-metal dichalcogenides [molybdenum disulfide (MoS_2), tungsten disulfide (WS_2), etc.], are promising materials for microelectronics because of their strong mechanical integrity derived from the covalent-bonded network and their ability to integrate or to adhere to dielectric substrates. The interactions between thin films and substrates affect the electrical, chemical, and mechanical properties of thin-film materials and their applications.[1,2] Therefore, thin-film adhesion is an indispensable property not only for microelectronics on substrates but also for emerging technologies such as the heterostructures of 2DN devices.[3] The adhesion energies of thin films on dissimilar rigid substrates have been measured qualitatively (tape tests)[4] and was used to compare the adhesion of different films and quantitatively with numerous methods,[5] like scratch testing,[6,7] four-point bend testing,[8] stressed overlayers,[9] and nanoindentation.[10] Nevertheless, it has been a challenge to measure the adhesion of 2DNs on substrates, because the thin 2DNs are difficult to handle and prone to damage in conventional tests. Recently, new methods for the adhesion measurement of graphene on various substrates have been reported, such as pressurized blisters,[11] nanoparticle blisters,[12] and mechanical delamination.[13]

In general, films that will adhere to the substrate are desired, although spontaneous delamination may occur at any time because of residual stress-induced crack growth, wrinkle formation, and other separations between the thin film and substrate.[14] These delamination-motivated corrugations (wrinkles, crumples, and folds) in free 2DNs result in local strain distribution and curvature-induced rehybridization, which modify (a) the electronic structure, local charge distribution, dipole moment, and optical properties of 2DNs and (b) the local chemical potential. These modified properties can then be applied toward electronics, self-assembly of complex structures, nanoelectromechanics, and bioelectronics.[15] Therefore, it is critical to control the physical attributes, like wrinkle formation of 2DNs, to further modify the properties and applications. These wrinkle attributes are governed by the adhesion between thin films and supporting substrates.

Wrinkles on soft materials have been shown in previous studies.[16−19] Because soft materials are stretchable, wrinkles can be formed on soft substrates by transferring MoS_2 to a prestretched surface and releasing the stretch after thin-film deposition. It is difficult to form wrinkles on unstretchable rigid substrates. However, direct measurement of the adhesion

Received: December 16, 2016
Accepted: January 26, 2017
Published: January 26, 2017

DOI: 10.1021/acsami.6b16175
ACS Appl. Mater. Interfaces 2017, 9, 7812−7818

energy of a MoS_2 solid on substrates [silicon dioxide (SiO_2), silicon nitride (Si_3N_4), etc.] is important to better understand the wrinkle formation mechanism and control the mechanical release of the wrinkles in MoS_2 for electrical device application. However, such measurements have not been reported yet. Here, we produced wrinkles on a rigid surface by a Scotch tape peeling method, and a range of the adhesion energy values of MoS_2 thin film on a SiO_2 substrate was estimated by the Young's equation. A definite energy model was built to quantitatively measure the MoS_2 adhesion energy on SiO_2 and a Si_3N_4 surface. Comprehensive experiments and analysis were conducted to prove the validity of this mechanical energy model.

EXPERIMENTS AND METHODS

The study was conducted on silicon dioxide (SiO_2) and silicon nitride (Si_3N_4) substrates. The wafers were diced into approximately 1 × 1 cm^2 pieces, cleaned with acetone and isopropyl alcohol, and dried in air. Molybdenum disulfide (MoS_2) sheets were mechanically cleaved from the surface of a MoS_2 block (SPI) by Scotch tape peeling. To transfer the MoS_2 flakes on SiO_2, the tape (width of 1 cm) was lightly pressed onto the MoS_2 block (about 0.3 × 0.3 cm^2) and then separated slowly. This transferred thick flakes to the tape. The tape with the flakes was then brought into contact with the SiO_2 or Si_3N_4 substrate under dry conditions, and a slight pressure was applied for 10 s. Finally, the pressure was released, and the tape was quickly peeled off, resulting in MoS_2 deposition on the substrate. The adhesion forces (van der Waals) pulled the MoS_2 sheets into intimate contact with the substrates. Mechanical equilibrium was reached when MoS_2 contracted to form a wrinkle in MoS_2, as shown in Figure 1a,b. The interfacial adhesion energies of MoS_2 and the substrates were found by measuring the wrinkle dimensions (amplitude, wavelength, and thickness of the MoS_2 flakes). Atomic force microscopy (AFM) was applied to measure the topography of the substrate and MoS_2 flake thickness and wrinkle attributes. The resolution of AFM in the z direction was 0.1 nm (for the thickness and amplitude), and in the lateral direction, it was about 10 nm (for the wavelength). Strain measurement was performed in Raman spectroscopy.

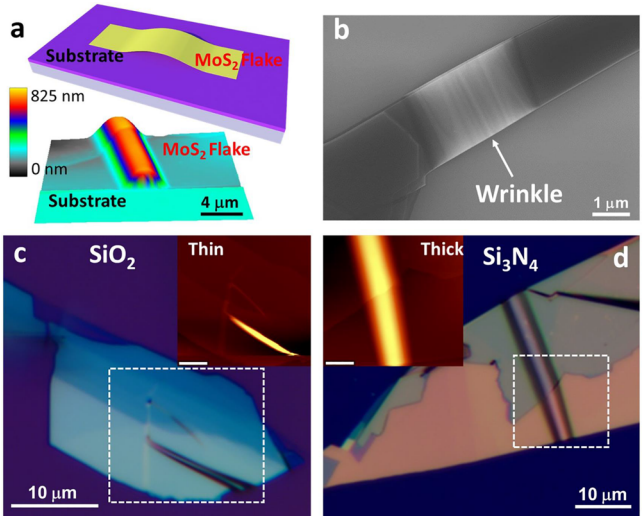

Figure 1. Typical wrinkled MoS_2 on substrates. (a) Schematic of a wrinkled MoS_2 flake on a substrate and AFM 3D image of a wrinkled MoS_2 flake. (b) FESEM characterization image of a typical wrinkled MoS_2 on a substrate. (c) Optical image of MoS_2 flakes on a SiO_2 substrate. Inset: AFM image of the dashed square area in part c. The thickness of the wrinkled part of MoS_2 is 17 nm, and the scale bar in the insert is 4 μm. (d) Optical image of MoS_2 flakes on a Si_3N_4 substrate. Inset: AFM image of the dashed square area in part d. The thickness of the upper wrinkled part of MoS_2 is 80 nm, and the scale bar in the inset is 4 μm.

RESULTS AND DISCUSSION

The adhesion of MoS_2 on the substrate causes the separation of thin MoS_2 flakes from the bulk MoS_2 in the mechanical exfoliation process. The curvature in wrinkled MoS_2 flakes leads to bending and delamination of MoS_2 on the substrate. The interplay between adhesion and bending energies results in stable, partially separated, wrinkled MoS_2 on the substrates. Therefore, these wrinkles' attributes are used to calculate the adhesion energy of MoS_2 on the substrates. Typical wrinkled MoS_2 films on substrates, as observed under field-emission scanning electron microscopy (FESEM), are shown in Figure 1b. Because the FESEM micrograph contrast corresponds to electron scattering due to surface curvature and electron density, the wrinkled region is brighter than the flat regions.[20] Wrinkled MoS_2 are formed on both SiO_2 and Si_3N_4 surfaces, as shown in Figures 1c,d and 2. The thickness of the MoS_2 sheet is shown quantitatively in the AFM images, and they also could be qualitatively distinguished from the color in the optical images in Figure 1c,d. The wrinkles' size (amplitude and wavelength) on the relatively thin MoS_2 (thickness = 17 nm; Figure 1c) is smaller than the wrinkles on the thick MoS_2 flake (thickness = 80 nm; Figure 1d).

The height profiles of the wrinkles and the thicknesses of the MoS_2 flakes are shown in Figure 2. It should be noted that the horizontal axis is in the micrometer scale and the vertical axis is in the nanometer scale in the crossline scan of the AFM image. Therefore, wrinkles would have a much smaller actual height/width ratio if the horizontal and vertical axes were to scale. The wrinkles are "smooth" (small curvature) and symmetric, which is an important assumption in our model (as shown latter) because part of the bending energy will be counteracted in the sharp and asymmetric region and weaken the adhesion of the interface.

Thermodynamically, the work of the adhesion of the interface is the amount of energy required to separate the thin film from the substrate and form free surfaces of thin film:[21]

$$W = \gamma_f + \gamma_s + \gamma_{fs} \quad (1)$$

γ_f and γ_s are the surface energies of the MoS_2 film and substrate, respectively, and γ_{fs} is the adhesion energy for the film/substrate interface. Contact-angle measurement is the most convenient and rapid method to probe the surface energy. Therefore, eq 1 is often rewritten as Young's equation:

$$\gamma_{fs} = \gamma_s - \gamma_f \cos\theta \quad (2)$$

where θ is the contact angle, as shown in Figure 3a, and $150^\circ \leq \theta < 180^\circ$ from the experimental data in our case. The surface energies of SiO_2 (γ_{SiO_2} = 0.115−0.200 J m^{2-})[11] and MoS_2 (γ_{MoS_2} = 0.0465 J m^{2-})[22] give that the MoS_2/SiO_2 interfacial energy γ_{MoS_2/SiO_2} = 0.155−0.246 J m^{-2} from eq 2. However, there are no reliable data for the surface energy of Si_3N_4 ($\gamma_{Si_3N_4}$) at room temperature, which leads to an unavailable estimation for γ_{MoS_2/Si_3N_4} in Young's equation.

The formation of wrinkles is a consequence of the interplay between the bending energy of the MoS_2 flakes and the interface adhesion energy,[18] as shown in Figure 3b. The adhesion energy of the MoS_2 flakes can be measured accurately

DOI: 10.1021/acsami.6b16175
ACS Appl. Mater. Interfaces 2017, 9, 7812−7818

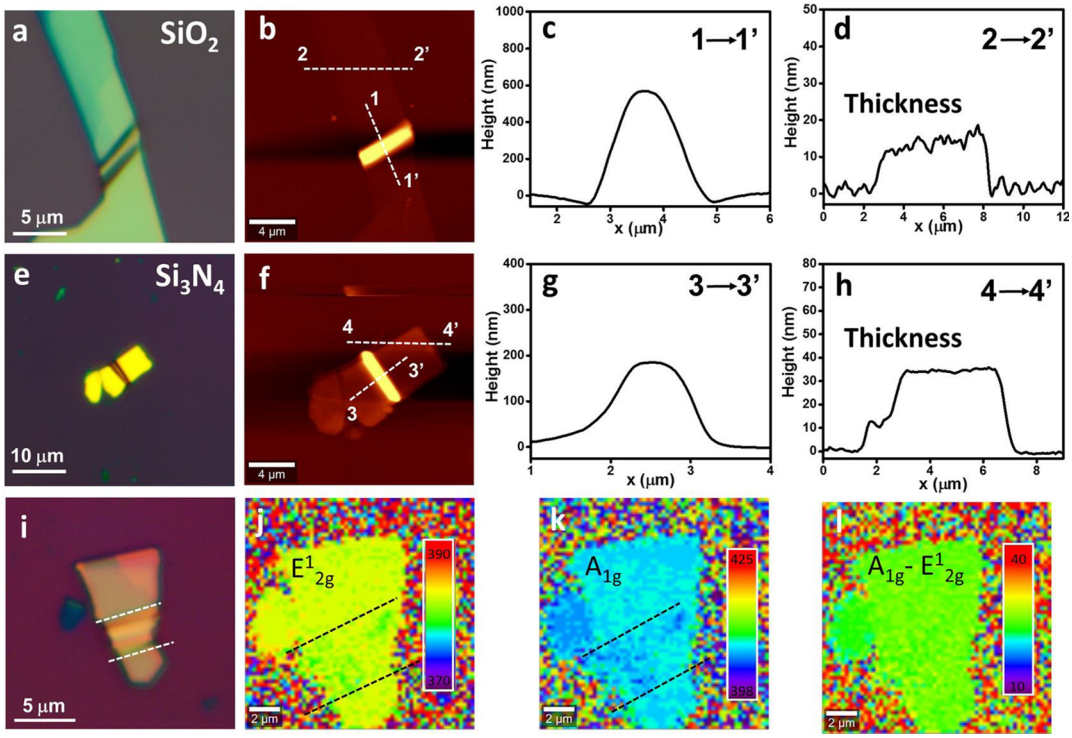

Figure 2. Characterizations of wrinkled MoS_2. (a) Optical image of a MoS_2 flake on a SiO_2 substrate. (b) AFM image of part a. (c and d) Height profiles of the corresponding dashed lines in part b. (e) Optical image of a MoS_2 flake on a Si_3N_4 substrate. (f) AFM image of part e. (g and h) Height profiles of the corresponding dashed lines in part f. Note that the vertical scales (y axis) in the profiles are in nanometers and the horizontal scales (x axis) are in micrometers. (i) Typical optical image of wrinkled MoS_2 flakes on SiO_2. The region between the white dashed lines is the wrinkled region. (j and k) Raman position mapping of the E^1_{2g} and A_{1g} modes, respectively. Both the E^1_{2g} and A_{1g} mode peaks in the wrinkled regions (between the two dashed lines) have red shifts (low Raman position shifts) compared to that of MoS_2 in a flat region. (l) Raman position difference between the E^1_{2g} and A_{1g} modes. No obvious color transition from flat to wrinkled MoS_2 indicates that there is no strong axial compressive strain or separation between the MoS_2 layers in the wrinkled region. The units for the scale bars in parts j–l are reciprocal centimeters.

from the thickness of the flakes and the size of the wrinkles. We assume that the van der Waals forces between MoS_2 layers are strong and sufficiently enough to adhere to each other, so no significant sliding or delamination occurs in the MoS_2 layers, as shown in Figure 2l and explained later.[11]

The total energy (U_T) of the wrinkled MoS_2 system can be represented as the following equation: $U_T = U_B + U_A + U_S$, where U_B is the bending energy for wrinkles in the MoS_2 sheet, U_A is the adhesion energy of MoS_2 on the substrates, and U_S is the interlayer sheet energy in the MoS_2 wrinkles. Assuming that the wavelength of a wrinkle is constant in the y direction, as shown in Figure 3a, therefore, the wrinkle energy analysis can be simplified to a two-dimensional model in the xz plane. The units of all energies are joules per meter. The corresponding out-of-plane displacement in the wrinkled MoS_2 sheet can be simplified as $z = \frac{A}{2}\left[1 + \cos\left(\frac{2\pi x}{\lambda}\right)\right]$,[23,24] which satisfies the boundary condition of zero slope at the two ends ($x = \pm\frac{1}{2}\lambda$), where A is the amplitude and λ is the wavelength of the wrinkle, respectively. The bending energy can be written as $U_B = \frac{\pi^4 E t^3 A^2}{12\lambda^3}$,[23] where E is Young's modulus of the MoS_2 sheet ($E = 1.99 \times 10^{11}$Pa)[25] and t is the thickness of the sheet. The adhesion energy $U_A = -\gamma(L - \lambda)$, where γ is the adhesion energy between MoS_2 and the substrate per unit area (J m^{-2}), L is the projected length of the wrinkled MoS_2 on substrates (the xy plane in the x direction), and L_0 is the original length of the wrinkled MoS_2 sheet in the x direction. The sheet energy $U_S = \frac{1}{2}EtL\left(\frac{\pi^2 A^2}{4L\lambda} - |\Delta|^2\right)$ with $\Delta = (L - L_0)/L$ as the plane strain.[18,26] However, the sheet energy in our case is negligible, as shown in the Raman strain study in Figure 2. In the wrinkled region, the two most prominent Raman peaks, the E^1_{2g} (near 384 cm^{-1}) and A_{1g} (near 405 cm^{-1}) modes, are red-shifted (the vibrations soften), as shown in Figure 2j,k. These red shifts indicate the strain in the plane of the MoS_2 flake and the existence of wrinkles. Further, there is no obvious change of the difference between the E^1_{2g} and A_{1g} modes in the wrinkled region compared to that of the flat part, as shown in Figure 2l. This means no separation between the MoS_2 layers in the wrinkled region. Therefore, the sheet energy U_S can be ignored in the total energy. The linear total energy can be rewritten as

$$U_T = U_B + U_A = \frac{\pi^4 E t^3 A^2}{12\lambda^3} - \gamma(L - \lambda) \tag{3}$$

Minimizing U_T with respect to A and λ leads to $A = \frac{2\lambda}{\pi}\sqrt{\left(|\Delta| - \frac{\pi^2 t^2}{3\lambda^2}\right)\frac{L}{\lambda}}$ and $\frac{\pi^2 t^3}{3\lambda^3}\left(\frac{\pi^2 t^2}{3\lambda^2} - |\Delta|\right) + \frac{\gamma}{2EL} = 0$. Assuming that $|\Delta| >> \frac{\pi^2 t^2}{3\lambda^2}$ and $|\Delta| - \frac{\pi^2 t^2}{3\lambda^2} \sim |\Delta|$ yields

$$\frac{\lambda}{t} = \sqrt[3]{\frac{2\pi^2 E(L_0 - L)}{3\gamma}} \tag{4}$$

DOI: 10.1021/acsami.6b16175
ACS Appl. Mater. Interfaces 2017, 9, 7812–7818

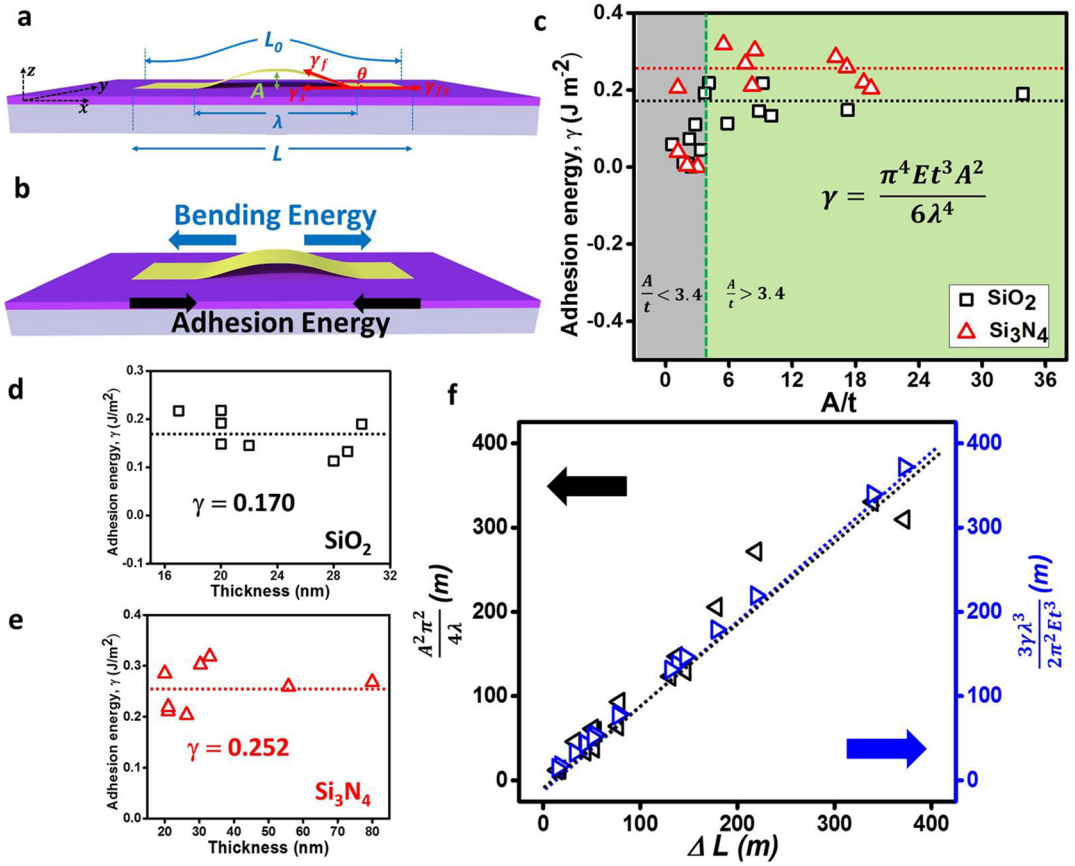

Figure 3. Wrinkled MoS_2 on the substrate and adhesion energy calculation and analysis. (a) Schematic of the wrinkled MoS_2. L_0 is the original length of MoS_2, L is the project length of the wrinkled MoS_2 on the substrate, A and λ stand for the amplitude and wavelength of the wrinkle, respectively, red arrows stand for the surface energies at the contact region, γ_f and γ_s are the surface energies of the MoS_2 film and substrate, respectively, γ_{fs} is the energy for the film/substrate interface, and θ is the contact angle. (b) Schematic of the energy distribution in wrinkled MoS_2. The sheet energy is not shown here. (c) Adhesion energy calculation of MoS_2 on the SiO_2 (black squares) and Si_3N_4 (red triangles) surfaces versus the normalized amplitude A/t. The green dashed line is $A/t = 3.4$. The gray area has $A/t < 3.4$, and the green area has $A/t > 3.4$. The black and red dashed lines are the average of the respective data for SiO_2 and Si_3N_4 in the green area. (d and e) Thickness dependence of the adhesion energies of MoS_2 on SiO_2 and Si_3N_4. The value of the black dashed line is $\gamma = 0.170$, and the value of the red dashed line is $\gamma = 0.252$. (f) Length-scale parameters $3\gamma\lambda^3/2\pi^2Et^3$ (blue) and $A^2\pi^2/4\lambda$ (black) versus ΔL. The units of both length-scale parameters and ΔL are meters.

$$A = \frac{2\lambda}{\pi}\sqrt{\frac{L_0 - L}{\lambda}} \tag{5}$$

Combining eqs 4 and 5, we obtain

$$\frac{A}{\lambda} = \frac{2}{\pi}\sqrt{\frac{\sqrt[3]{L_0 - L}^2}{t}\sqrt[3]{\frac{3\gamma}{2\pi^2 E}}} \tag{6}$$

Therefore,

$$\gamma = \frac{\pi^4 E t^3 A^2}{6\lambda^4} \tag{7}$$

The calculation results of the adhesion energies for MoS_2 on SiO_2 and Si_3N_4 are shown in Figure 3c. However, it should be noted that eqs 4−7 are also based on the condition $|\Delta| \gg \frac{\pi^2 t^2}{3\lambda^2}$. The axial compressive strain $\Delta = \frac{A^2\pi^2}{4\lambda L}$ is given by rewriting eq 5 and $\frac{A^2\pi^2}{4\lambda L} \gg \frac{\pi^2 t^2}{3\lambda^2}$. From the experimental data, we know that L is on the scale of 10 μm and λ is on the scale of 1 μm; this leads to $\frac{A^2}{t^2} \gg \frac{L}{\lambda} \approx 10$, and the value of normalized amplitude A/t should be greater than 3.4 for the validity of $|\Delta| \gg \frac{\pi^2 t^2}{3\lambda^2}$. Therefore, the data with $A/t \geq 3.4$ are more suitable for calculation of the adhesion energy in our model. The adhesion energies for a MoS_2 nanoscale thin film on SiO_2 and Si_3N_4 are 0.170 ± 0.033 and 0.252 ± 0.041 J m^{-2}, respectively. This adhesion energy for the MoS_2/SiO_2 interface closely agrees with the value that we estimated through Young's equation (eq 2).

Calculations of the adhesion energies based on selected data versus the thickness of the thin film are shown in Figure 3d (SiO_2) and 3e (Si_3N_4). The results show a thickness independence in a broad range (thickness larger than 15 nm) for both substrates. This validity is guaranteed by the normalized amplitude condition ($A/t \geq 3.4$). Rewriting eq 4 to a length-scale parameter of $3\gamma\lambda^3/2\pi^2Et^3$ and eq 5 to the same length-scale parameter $\Delta L = A^2\pi^2/4\lambda$, therefore, we have

$$\frac{3\gamma\lambda^3}{2\pi^2 E t^3} = \frac{A^2\pi^2}{4\lambda} \tag{8}$$

Equation 8 can also be used to verify the value of the adhesion energies; a comparison of the parameters on the two sides of eq 8 is shown in Figure 3e. The overlap of linear fittings for the experiments ($3\gamma\lambda^3/2\pi^2Et^3$) and theory ($A^2\pi^2/4\lambda$) shows that our data are well fit to our model.

DOI: 10.1021/acsami.6b16175
ACS Appl. Mater. Interfaces 2017, 9, 7812−7818

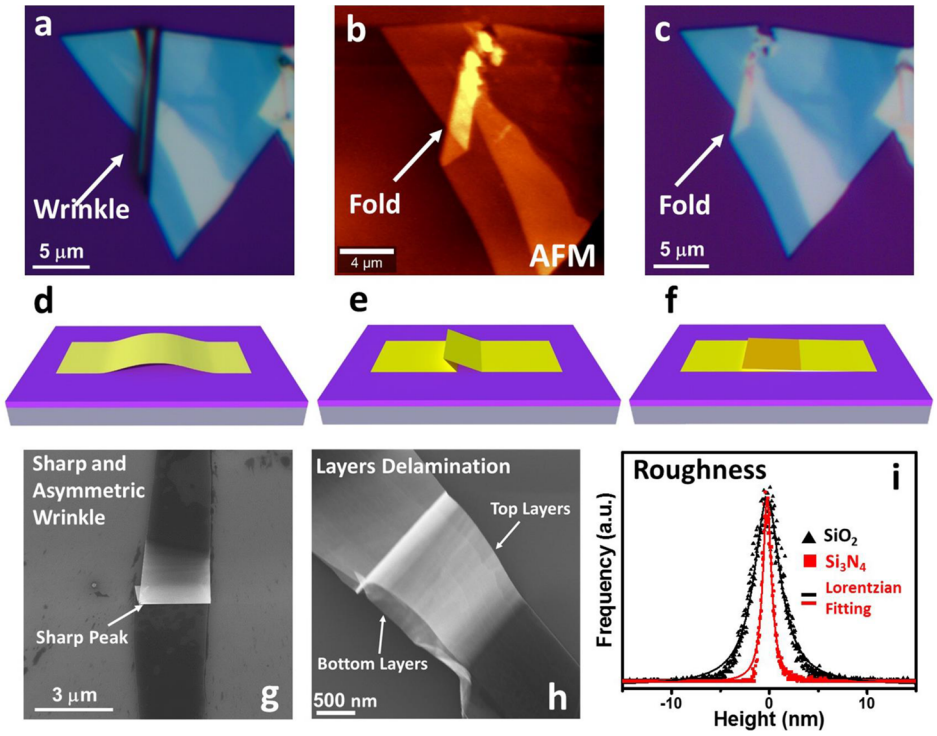

Figure 4. MoS_2 wrinkling on SiO_2 and Si_3N_4 surface mechanism analysis. (a) Optical image of the thin MoS_2 flakes on the SiO_2 surface right after mechanical exfoliation. The dark bar region is the wrinkle. (b) AFM image of the same area in part a. The wrinkle collapsed and formed a fold in the scanning process. The thickness of the flake in the wrinkled region is 10 nm. (c) Optical image of the thin MoS_2 flakes on the SiO_2 surface after scanning. The wrinkles collapsed and disappeared, and the fold was formed. (d–f) Schematics of symmetrical, asymmetrical, and folder wrinkles on substrates. (g) SEM image of a sharp and asymmetrical wrinkled MoS_2. (h) SEM image of a layered delamination in MoS_2. The top layers are thin and wrinkled and delaminated from the bottom layers. (i) Surface roughness of SiO_2 and Si_3N_4 substrates compared by height-histogram analysis of the AFM data on the two surfaces. The solid lines are the Lorentzian fits for the roughness data. The widths of the peaks represent the surface height distribution.

Additionally, transformations of eqs 4 and 5 also give the plane strain as

$$\Delta = \frac{A^2\pi^2}{4\lambda L} = \frac{3\gamma\lambda^3}{2\pi^2 E t^3 L} \tag{9}$$

This means that for certain thicknesses of the thin film on substrates (known as t and γ) that formed wrinkles, two-dimensional size characteristics, the wavelength of the wrinkles (λ) and length of the thin film (L), but not the three-dimensional measurement, the amplitude (A), are needed for the plane strain (Δ) measurement. Because the amplitude measurement is a slow, expensive, and destructive process, as shown later, eq 9 will provide a fast, low-cost, and damage-free plane strain measurement approach for thin 2DNs.

MECHANISMS AND ANALYSIS

The adhesion is affected by the film thickness, microstructure, chemistry, and test temperature.[21] For the adhesion study on graphene, monolayer graphene showed larger adhesion than the two-to-five-layer graphene; this was attributed to the extreme flexibility of graphene, which allowed it to conform to the topography of the substrates, thus making its interaction with the substrate more liquidlike than solidlike (more rigid and less accommodative to the substrate surface).[11] The result shown in Figure 3d,e does not mean that the adhesion is thickness-independent for any thickness of the MoS_2 film. Ultrathin (monolayers) MoS_2 may have higher adhesions on substrates than MoS_2 multilayers because of higher flexibility.[11] However, this effect in MoS_2 is expected to be reduced because of the three-atom-thick network in monolayer MoS_2 instead of the one atomic layer in monolayer graphene. The liquidlike interaction is expected to be absent for a thickness larger than 15 nm (20 layers). Thinner films fit better in our model, as shown in our calculation; the value of $\pi^2t^2/3\lambda^2$ decreased and the value of the normalized amplitude A/t increased for the thinner MoS_2 film. However, thin layers of MoS_2 (below 10 nm) are not applicable for the adhesion calculation because of the reduced bending rigidity of the thin layers of the MoS_2 sheet. In our case, the thin-film wrinkles will collapse and form folds, especially in the AFM process, which are unstable, with one side collapsed on the other side of the wrinkles. This formation of folds leads to smaller adhesion energy in the calculation because the collapse leads to smaller wrinkle amplitude but larger wavelength, as shown in Figure 4a–c. In this case, the symmetrical wrinkles are expected to experience external forces (AFM measurement), then transform to asymmetrical and sharp wrinkles, and collapse into folded wrinkles in the end, as shown in Figure 4d–f.

Further, small wrinkles, even on relatively thick flakes, are unreliable in the calculation of the adhesion because the values of the normalized amplitude A/t would be smaller than 3.4. Additionally, small wrinkles do not fit our model and can form for several reasons. One is that only partial flake layers may be involved in the formation of wrinkles: only a few top layers are wrinkled, and these wrinkles are supported on the bottom layers of MoS_2 instead of the substrate, as shown in Figure 4h. The top layers are very thin and partially delaminated from the

DOI: 10.1021/acsami.6b16175
ACS Appl. Mater. Interfaces 2017, 9, 7812–7818

bottom layers, which is visible through the top layers (Figure 4h). The wrinkle is a consequence of the bending of the top layers and adhesion between MoS_2 layers, which can be applied to the study of the interlayer adhesion. Another reason could be that the contamination at the interface between substrates and flakes could result in deformation of the flakes. Further, the line defects and deformations in the bulk MoS_2 can also induce wrinkle-like topography of the surface of the flakes, as shown in Figure S1 (see the Supporting Information). Because part of the bending energy is partially counteracted in the sharp and asymmetric region, the adhesion is weak at the interface, as shown in Figure 4g. This would result in a false high adhesion in the calculation with eq 7. Further, these wrinkles cannot be eliminated through the condition $A/t \geq 3.4$ because they have distorted high amplitudes compared to the smooth wrinkles. These types of wrinkles can be excluded from the AFM height profiles, as shown in Figure S2 (see the Supporting Information). All of these situations were avoided in the data collection for the adhesion calculation.

These values of adhesion energy of MoS_2 on SiO_2 are smaller than those of the previous study[11] on graphene sheet on SiO_2, which can be attributed to the MoS_2 flakes being less flexible to conform to the topography of the substrate, especially for the relatively "thick" MoS_2 flakes used in our study. On the other hand, the MoS_2 flakes show larger adhesion on the Si_3N_4 surface than the SiO_2 surface. This may be caused by the difference in roughness between these two surfaces. The roughness of the SiO_2 and Si_3N_4 surface can be detected by the AFM, as shown in Figure 4i. The Si_3N_4 surface is smoother than the SiO_2 surface. Theoretical studies have indicated that adhesion energy increases with a decrease in the substrate's roughness (idealized sinusoidal profiles).[27] Here, Si_3N_4 is expected to make a closer and more intimate contact with MoS_2 than SiO_2.

In conclusion, we have demonstrated that a wrinkled MoS_2 can be used to determine the adhesion energy between MoS_2 and rigid substrates (SiO_2 and Si_3N_4). The adhesion energies of 0.170 ± 0.033 J m^{-2} for MoS_2 on SiO_2 and 0.252 ± 0.041 J m^{-2} for MoS_2 on Si_3N_4 were obtained. The different values on these two substrates are attributed to the roughness of the surfaces. This method is suitable for wrinkles with $A/t \geq 3.4$. Wrinkles in an ultrathin film (<10 nm) were not stable in the AFM measurement. We also propose a method to measure the strain in three-dimensional wrinkles without measuring the amplitude of the wrinkles. Further, the plane strain measurement for wrinkles on an ultrathin film can be attained without damaging the wrinkles. The results shown here may be extended to study the surface interactions, 2DN interfacial properties, and thin-film device fabrication processes.

■ ASSOCIATED CONTENT

Supporting Information

The Supporting Information is available free of charge on the ACS Publications website at DOI: 10.1021/acsami.6b16175.

Small wrinkles on the thick MoS_2 sheet (Figure S1) and sharp and asymmetric wrinkles on a MoS_2 sheet (Figure S2) (PDF)

■ AUTHOR INFORMATION

Corresponding Author

*E-mail: vikasb@uic.edu.

ORCID

Enlai Gao: 0000-0003-1960-0260

Vikas Berry: 0000-0002-1102-1996

Notes

The authors declare no competing financial interest.

■ ACKNOWLEDGMENTS

V.B. acknowledges financial support from National Science Foundation (Grants CMMI-1503681 and CMMI-1030963) and University of Illinois at Chicago. Thanks to Yue Liu for help with the schematics. Thanks to Dr. Sanjay Behura for valuable discussion.

■ REFERENCES

(1) Zhang, K.; Feng, S.; Wang, J.; Azcatl, A.; Lu, N.; Addou, R.; Wang, N.; Zhou, C.; Lerach, J.; Bojan, V.; Kim, M. J.; Chen, L.-Q.; Wallace, R. M.; Terrones, M.; Zhu, J.; Robinson, J. A. Manganese Doping of Monolayer MoS2: The Substrate Is Critical. *Nano Lett.* **2015**, *15* (10), 6586−6591.

(2) Behura, S.; Nguyen, P.; Che, S.; Debbarma, R.; Berry, V. Large-Area, Transfer-Free, Oxide-Assisted Synthesis of Hexagonal Boron Nitride Films and Their Heterostructures with MoS2 and WS2. *J. Am. Chem. Soc.* **2015**, *137* (40), 13060−13065.

(3) Britnell, L.; Gorbachev, R. V.; Jalil, R.; Belle, B. D.; Schedin, F.; Mishchenko, A.; Georgiou, T.; Katsnelson, M. I.; Eaves, L.; Morozov, S. V.; Peres, N. M. R.; Leist, J.; Geim, A. K.; Novoselov, K. S.; Ponomarenko, L. A. Field-Effect Tunneling Transistor Based on Vertical Graphene Heterostructures. *Science* **2012**, *335* (6071), 947−950.

(4) Hull, T. R.; Colligon, J. S.; Hill, A. E. Measurement of Thin Film Adhesion. *Vacuum* **1987**, *37* (3), 327−330.

(5) Cordill, M. J.; Bahr, D. F.; Moody, N. R.; Gerberich, W. W. Recent Developments in Thin Film Adhesion Measurement. *IEEE Trans. Device Mater. Reliab.* **2004**, *4* (2), 163−168.

(6) Rickerby, D. S. A Review of the Methods for the Measurement of Coating-Substrate Adhesion. *Surf. Coat. Technol.* **1988**, *36* (1), 541−557.

(7) Thouless, M. D. An Analysis of Spalling in the Microscratch Test. *Eng. Fract. Mech.* **1998**, *61* (1), 75−81.

(8) Dauskardt, R. H.; Lane, M.; Ma, Q.; Krishna, N. Adhesion and Debonding of Multi-Layer Thin Film Structures. *Eng. Fract. Mech.* **1998**, *61* (1), 141−162.

(9) Bagchi, A.; Lucas, G. E.; Suo, Z.; Evans, A. G. A New Procedure for Measuring the Decohesion Energy for Thin Ductile Films on Substrates. *J. Mater. Res.* **1994**, *9* (7), 1734−1741.

(10) De Boer, M. P.; Gerberich, W. W. Microwedge Indentation of the Thin Film Fine line—I. Mechanics. *Acta Mater.* **1996**, *44* (8), 3169−3175.

(11) Koenig, S. P.; Boddeti, N. G.; Dunn, M. L.; Bunch, J. S. Ultrastrong Adhesion of Graphene Membranes. *Nat. Nanotechnol.* **2011**, *6* (9), 543−546.

(12) Zong, Z.; Chen, C. L.; Dokmeci, M. R.; Wan, K. T. Direct Measurement of Graphene Adhesion on Silicon Surface by Intercalation of Nanoparticles. *J. Appl. Phys.* **2010**, *107* (2), XXX DOI: 10.1063/1.3294960.

(13) Yoon, T.; Shin, W. C.; Kim, T. Y.; Mun, J. H.; Kim, T.-S.; Cho, B. J. Direct Measurement of Adhesion Energy of Monolayer Graphene As-Grown on Copper and Its Application to Renewable Transfer Process. *Nano Lett.* **2012**, *12* (3), 1448−1452.

(14) Annett, J.; Cross, G. L. W. Self-Assembly of Graphene Ribbons by Spontaneous Self-Tearing and Peeling from a Substrate. *Nature* **2016**, *535* (7611), 271−275.

(15) Deng, S.; Berry, V. Wrinkled, Rippled and Crumpled Graphene: An Overview of Formation Mechanism, Electronic Properties, and Applications. *Mater. Today* **2016**, *19* (4), 197−212.

(16) Castellanos-Gomez, A.; Roldán, R.; Cappelluti, E.; Buscema, M.; Guinea, F.; van der Zant, H. S. J.; Steele, G. A. Local Strain

Engineering in Atomically Thin MoS2. *Nano Lett.* **2013**, *13* (11), 5361−5366.
(17) Yang, S.; Wang, C.; Sahin, H.; Chen, H.; Li, Y.; Li, S.-S.; Suslu, A.; Peeters, F. M.; Liu, Q.; Li, J.; Tongay, S. Tuning the Optical, Magnetic, and Electrical Properties of ReSe2 by Nanoscale Strain Engineering. *Nano Lett.* **2015**, *15* (3), 1660−1666.
(18) Wang, B.; Wang, S. Adhesion-Governed Buckling of Thin-Film Electronics on Soft Tissues. *Theor. Appl. Mech. Lett.* **2016**, *6* (1), 6−10.
(19) Deng, S.; Gao, E.; Wang, Y.; Sen, S.; Sreenivasan, S. T.; Behura, S.; Král, P.; Xu, Z.; Berry, V. Confined, Oriented, and Electrically Anisotropic Graphene Wrinkles on Bacteria. *ACS Nano* **2016**, *10* (9), 8403−8412.
(20) Castle, J. E.; Zhdan, P. A. Characterization of Surface Topography by SEM and SFM: Problems and Solutions. *J. Phys. D: Appl. Phys.* **1997**, *30* (5), 722.
(21) Volinsky, A. A.; Moody, N. R.; Gerberich, W. W. Interfacial Toughness Measurements for Thin Films on Substrates. *Acta Mater.* **2002**, *50* (3), 441−466.
(22) Gaur, A. P. S.; Sahoo, S.; Ahmadi, M.; Dash, S. P.; Guinel, M. J.-F.; Katiyar, R. S. Surface Energy Engineering for Tunable Wettability through Controlled Synthesis of MoS2. *Nano Lett.* **2014**, *14* (8), 4314−4321.
(23) Vandeparre, H.; Piñeirua, M.; Brau, F.; Roman, B.; Bico, J.; Gay, C.; Bao, W.; Lau, C. N.; Reis, P. M.; Damman, P. Wrinkling Hierarchy in Constrained Thin Sheets from Suspended Graphene to Curtains. *Phys. Rev. Lett.* **2011**, *106* (22), 224301.
(24) Deng, S.; Berry, V. Increased Hierarchical Wrinklons on Stiff Metal Thin Film on a Liquid Meniscus. *ACS Appl. Mater. Interfaces* **2016**, *8* (37), 24956−24961.
(25) Li, T. Ideal Strength and Phonon Instability in Single-Layer MoS${}_{2}$. *Phys. Rev. B: Condens. Matter Mater. Phys.* **2012**, *85* (23), 235407.
(26) Wang, S.; Xiao, J.; Song, J.; Ko, H. C.; Hwang, K.-C.; Huang, Y.; Rogers, J. A. Mechanics of Curvilinear Electronics. *Soft Matter* **2010**, *6* (22), 5757−5763.
(27) Aitken, Z. H.; Huang, R. Effects of Mismatch Strain and Substrate Surface Corrugation on Morphology of Supported Monolayer Graphene. *J. Appl. Phys.* **2010**, *107* (12), 123531.

DOI: 10.1021/acsami.6b16175
ACS Appl. Mater. Interfaces 2017, 9, 7812−7818